Inorg. Chem. **2009**, *48*, 4143−4153

Does the 4f Electron Configuration Affect Molecular Geometries? A Joint Computational, Vibrational Spectroscopic, and Electron Diffraction Study of Dysprosium Tribromide

Cornelis Petrus Groen,[†,‡] Zoltán Varga,[†] Mária Kolonits,[†] Kirk A. Peterson,[§] and Magdolna Hargittai*[,†]

Materials Structure and Modeling Research Group of the Hungarian Academy of Sciences, Budapest University of Technology and Economics, P.O. Box 91, 1521 Budapest, Hungary, and Department of Chemistry, Washington State University, Pullman, Washington 99164

Received December 8, 2008

The molecular geometry and vibrational frequencies of monomeric and dimeric dysprosium tribromide, $DyBr_3$ and Dy_2Br_6, together with the electronic structure of their ground and first few excited-state molecules were determined by high-level computations, electron diffraction, gas-phase infrared, and matrix isolation infrared and Raman spectroscopy. The effect of partially filled 4f orbitals and spin−orbit coupling on their structure was studied by computations. While the geometry of the monomer does not depend on the 4f orbital occupation, the bond angles of the dimer are noticeably influenced by it. The monomer is found to be planar from all methods; the suggested equilibrium bond length of the molecule (r_e) is 2.591(8) Å, while the thermal average distance (r_g) is 2.606(8) Å. Although the gas-phase $DyBr_3$ molecule is planar, it forms a complex with the matrix molecules in the matrix-isolation spectroscopic experiments, leading to the pyramidalization of the $DyBr_3$ unit. Our model calculations in this regard also explain the often conflicting results of computations and different experiments about the shape of lanthanide trihalides.

Introduction

There is considerable practical interest in lanthanide trihalide vapors because of their importance in several industrial processes. They are used, among others, in high-temperature extraction and separation processes for lanthanides,[1] in purification processes of nuclear waste,[2] and in high-pressure metal halide discharge lamps.[3] Dysprosium tribromide itself is one of the most important ingredients of metal halide discharge lamps.[4] Thermodynamic modeling is often applied to provide a better understanding of the complex chemical interactions that take place in these processes. The reliability of the predictions depends on the quality of the input data that are the molecular and spectroscopic constants of the gaseous species involved.

The shape of rare-earth trihalides has been a matter of controversy. Over the past 40 years numerous experimental studies have tried to determine whether these molecules are planar or pyramidal (see, e.g., refs 5 and 6 and references therein). All the experimental methods, gas-phase electron diffraction (ED), gas-phase infrared spectroscopy (IR), and matrix-isolation infrared (MI-IR) and Raman (MI-Ra) spectroscopy, suffer from limitations connected with the high temperature conditions necessary to perform the experiments.[6] These conditions do not only pose technical difficulties for the experiments, but, in the case of the gas-phase IR studies, they lead to the excitation of vibrational states and to broad band contours, making unambiguous symmetry assignments impossible.[7,8]

* To whom correspondence should be addressed. E-mail: hargittaim@mail.bme.hu.
† Budapest University of Technology and Economics.
‡ Current address: Urenco Nederland B. V., P.O. Box 158, 7600 AD Almelo, The Netherlands.
§ Washington State University.

(1) Uda, T.; Jacob, K. T.; Hirasawa, M. *Science* **2000**, *289*, 2326–2329.
(2) Merli, L.; Rorif, F.; Fuger, J. *Radiochim. Acta* **1998**, *82*, 3–9.
(3) Haverlag, M. *Phys. Scr.* **2005**, *T119*, 67–70.
(4) Markus, T.; Niemann, U.; Hilpert, K. *J. Phys. Chem. Solids* **2005**, *66*, 372–375.
(5) Hargittai, M. *Coord. Chem. Rev.* **1988**, *91*, 35–88.
(6) Hargittai, M. *Chem. Rev.* **2000**, *100*, 2233–2301.
(7) Kovács, A.; Konings, R. J. M.; Booij, A. S. *Chem. Phys. Lett.* **1997**, *268*, 207–212.
(8) Kovács, A.; Konings, R. J. M. *Vib. Spectrosc.* **1997**, *15*, 131–135.

10.1021/ic802340g CCC: $40.75
Published on Web 03/31/2009

The vibrational frequencies of matrix-isolated species are often shifted compared to their respective vapor-phase values and additional signals might appear because of matrix site effects; eventually leading to erroneous assignment of the symmetric stretch fundamental ν_1, and thus to erroneous conclusions regarding the molecular symmetry. MI-IR experiments of rare-earth trifluorides have often been interpreted with pyramidal geometry.[9] For the chlorides, bromides, and iodides, no convincing spectroscopic evidence for a deviation from the planar geometry has been found so far.

It is well-known that many properties of lanthanide trihalides, among them their bond lengths and the metal ionic radii, change monotonically along the lanthanide series; inferring that the 4f subshell does not have any influence on them. An earlier photoelectron spectroscopic study of several lanthanide trihalides indicated, indeed, that the 4f orbitals occupy a rather restricted thin shell well separated from the valence region[10] and this was later supported by quantum chemical calculations.[11] At the same time, a recent computational study indicated that the 4f electrons do participate in the bonding of LuF_3.[12] Therefore, we decided to investigate this question with up-to-date computational methods, to our knowledge for the first time for a lanthanide tribromide, following our experience with $DyCl_3$.[13]

Computational studies of the lanthanides have been carried out for a long time; they have been summarized, together with the experimental literature data, in refs 14 and 6. For some more recent work see, for example, refs 15 and 16. The possibilities for computational studies of molecules containing rare earth metal atoms have improved greatly in recent years. The new effective core potentials (ECPs, for references see the computational section), besides making the computations for molecules involving these huge atoms viable, also incorporate scalar relativistic effects. They do not, however, include spin−orbit (SO) effects by default, and our second goal with these computations was to check if these effects have any influence on the structural properties of molecules involving rare earth metals. There has been one systematic study of the lanthanide trifluorides and trichlorides investigating the effect of 4f electrons on their properties by Taketsugu et al.,[17] and they also investigated the effect of spin−orbit coupling on the properties of these molecules. Our study of $DyCl_3$ also addressed these questions.[13]

A Knudsen effusion mass spectrometric study of dysprosium tribromide concluded that appreciable amounts of dimeric molecules were also present in its vapor beside the monomers.[18] A previous electron diffraction study of $DyBr_3$,[19] however, found only monomeric molecules in the vapor; they concluded that the molecules are probably planar. The experimental information on the vibrational frequencies of $DyBr_3$ is limited to the asymmetric stretching fundamental, ν_3, from an argon-matrix study.[20] Quantum chemical calculations have been performed on $DyBr_3$ at different levels, two of them[15,21] using large-core, and the latest one[16] small-core, ECPs. Since one of our matrix spectra might be interpreted as having resulted from a slightly pyramidal molecule (vide infra), we carried out computations on the possible effects of the matrix molecules on the shape of a lanthanide trihalide by computing the structures of different $DyBr_3 \cdot Kr_n$ ($n = 1-4$) complexes. We also carried out an anharmonic vibrational analysis of the out-of-plane vibration of the molecule, to understand the disagreement over this frequency between the experiments and computations. Finally, we computed the geometry and frequencies of the dimeric Dy_2Br_6 molecule to aid the electron diffraction study.

Computational and Experimental Details

Computational Methodology. State-of-the-art computations on a lanthanide trihalide are rather complex and here only their most important aspects are presented; interested readers are referred to the Supporting Information for details. At the first stage of our computations the possible effect of the 4f electron configuration on the structure of the monomeric $DyBr_3$ molecule was checked. In the simplest picture, the $DyBr_3$ molecule can be considered to consist of an ionic interaction between three closed-shell Br^- anions and Dy in its +3 oxidation state. The relevant highest occupied and lowest unoccupied orbitals then consist of the seven 4f orbitals of Dy in which nine electrons are distributed. Considering all possible distributions of the nine 4f electrons in these seven orbitals, a total of 21 high spin, sextet electronic states are possible: 3 in A_2'', 6 in E′, and 3 in E″ in the D_{3h} symmetry trigonal planar arrangement, or 6 in each A_1, B_1, and B_2 and 3 in A_2 in a lower, C_{2v}-symmetry arrangement that might occur because of the Jahn−Teller distortion of degenerate trigonal planar states. In the present work, the simplest CASSCF(9/7) calculations have been carried out, in which all possible excitations of the nine electrons in the seven 4f orbitals are considered and all of the above states were averaged. All other orbitals were constrained to be doubly occupied. This treatment results in just one configuration state function per electronic state, that is, a state-averaged Hartree−Fock calculation. Subsequent MRCI (and MRCI+Q) calculations were also carried out with the same active space,[22−26] in which the 4s4p

(9) Hastie, J. W.; Hauge, R. H.; Margrave, J. L. *J. Less-Common Met.* **1975**, *39*, 309–334.
(10) Ruscic, B.; Goodman, G. L.; Berkowitz, J. *J. Chem. Phys.* **1983**, *78*, 5443–5467.
(11) Dolg, M. In *Encyclopedia of Computational Chemistry*; Schleyer, P. V., Allinger, N. L., Clark, T., Gasteiger, J., Schaefer, H. F. I., Schreiner, P. R., Eds.; Wiley: Chichester, 1998; p 1478.
(12) Clavaguera, C.; Dognon, J. P.; Pyykko, P. *Chem. Phys. Lett.* **2006**, *429*, 8–12.
(13) Lanza, G.; Varga, Z.; Kolonits, M.; Hargittai, M. *J. Chem. Phys.* **2008**, *128*, 074301.
(14) Kovács, A.; Konings, R. J. M. *J. Phys. Chem. Ref. Data* **2004**, *33*, 377–404.
(15) Perrin, L.; Maron, L.; Eisenstein, O. *Faraday Discuss.* **2003**, *124*, 25–39.
(16) Saloni, J.; Roszak, S.; Hilpert, K.; Miller, M.; Leszczynski, J. *Eur. J. Inorg. Chem.* **2004**, 1212–1218.
(17) Tsuchiya, T.; Taketsugu, T.; Nakano, H.; Hirao, K. *J. Mol. Struct.: THEOCHEM* **1999**, *462*, 203–222.
(18) Hilpert, K.; Miller, M.; Ramondo, F. *J. Chem. Phys.* **1995**, *102*, 6194–6198.
(19) Giricheva, N. I.; Shlykov, S. A.; Chernova, E. V.; Levina, Y. S.; Krasnov, A. V. *J. Struct. Chem.* **2005**, *46*, 991–997.
(20) Feltrin, A.; Cesaro, S. N. *High Temp. Mater. Sci.* **1996**, *35*, 203–214.
(21) Kovács, A. *J. Mol. Struct.* **1999**, *483*, 403–407.
(22) Knowles, P. J.; Werner, H. J. *Chem. Phys. Lett.* **1988**, *145*, 514–522.
(23) Werner, H. J.; Knowles, P. J. *J. Chem. Phys.* **1988**, *89*, 5803–5814.
(24) Blomberg, M. R. A.; Siegbahn, P. E. M. *J. Chem. Phys.* **1983**, *78*, 5682–5692.
(25) Langhoff, S. R.; Davidson, E. R. *Int. J. Quantum Chem.* **1974**, *8*, 61–72.

electrons of bromine and the 5s5p4f6s electrons of dysprosium were correlated, leading to just over 4 million variational parameters. In addition to the MRCI calculations, second-order multireference perturbation theory (CASPT2) calculations[27,28] were also carried out using the same active space as above. The effect on the equilibrium geometry because of correlation of the Br 3d electrons was also investigated at this level of theory. The possibility of having a C_{3v}-symmetry pyramidal arrangement in lanthanide trihalides has often come up in the literature; therefore, that symmetry was also checked. These optimizations always led to planar structures.

The pseudopotentials used in this study (vide infra) incorporate scalar relativistic effects but they do not automatically treat spin−orbit coupling, which might be considerable for a lanthanide trihalide. Therefore, we also looked into the possible effect of spin−orbit coupling on the structure of $DyBr_3$. These calculations utilized the effective one-electron operators that were parametrized with the pseudopotentials. The state interacting approach[29] with state-averaged CASSCF orbitals was used, which included the 21 sextet states noted above together with 18 quartet states (5 each in A_1, B_1, and B_2 symmetry and 3 in A_2 symmetry). This yielded a total of 200 spin−orbit coupled eigenstates.

As shown before,[17] static electron correlation is important for describing the 4f configuration mixing. On the other hand, dynamic correlation is essential for determining reliable geometrical and vibrational parameters.[13,30] Therefore, at the second stage of our computations, and in addition to the MRCI+Q calculations previously described, UHF-MP2 calculations were carried out with different ECP/basis set combinations on Dy. We also wanted to see which one of these gave the best agreement with the experiments. Three different effective core potentials (ECPs) were applied in these calculations, the shape-consistent Cundari and Stevens quasirelativistic ECP (46 electrons, $[Kr]d^{10}$)[31] and two types of energy-consistent quasirelativistic ECPs by the Stuttgart group.[32−34] The so-called "large-core" (LC) ECPs, in which the 4f electrons are considered as core (55 electrons) and the "small core" (SC - $[Ar]d^{10}$).[34] Obviously, the LC ECPs cannot be used to study the $4f^n$ orbital occupation.

On the basis of our experience with $DyCl_3$,[13] we used the two kinds of Stuttgart ECPs and the Cundari ECP for describing the dysprosium atom, with different associated basis sets. In basis **A** the Stuttgart LC ECP was augmented by a valence basis set[35] with a (6s6p5d)/[4s4p4d] + 2s1p1d contraction and extended with two f polarization functions.[36] The second basis (**B**) used the Cundari ECP and the corresponding valence basis set [3111,3111,111,52] with one additional g polarization function.[13] In our highest-level computations (Basis set **C**) the SC Stuttgart ECP was used with its associated segmented-contracted valence basis set (14s13p10d8f6g)/[10s8p5d4f3g] for Dy. In most of these calculations the diffuse-augmented aug-cc-pVTZ-PP[37] basis set (with its associated small core ECP) was used on the Br atoms, except in some cases where simply the cc-pVTZ-PP basis was used. The investigation of Br 3d correlation employed the aug-cc-pVTZ-PP basis set augmented with additional tight d and f functions.

The structure of the dimer molecule was also calculated at the MP2 level with all basis sets used for the monomer. In addition, CASSCF calculations with basis **C** were carried out where the 18 4f electrons of Dy were distributed in the 14 4f orbitals, that is, CASSCF(18/14). Natural bond orbital[38−41] and Wiberg[42] bond index analyses were also carried out for both species. Vibrational frequencies for the monomer were calculated with all bases used, while for the dimer we only used bases **A** and **B**. Computations have also been carried out for the dysprosium monobromide molecule with the LC basis set for Dy at the MP2 level (see Supporting Information, Table S1). We also carried out a series of calculations on the complexes formed by $DyBr_3$ and different numbers of krypton atoms. In these calculations the LC ECP was applied on Dy and the Stuttgart RLC ECPs for bromine[43] and krypton,[44] for details see Supporting Information.

Different program packages were used during the course of our study; Molpro[45] for the CASSCF and MRCI calculations, Gaussian 98[46] and Gaussian 03[47] for the MP2 calculations and Gamess[48] for the PT2-VSCF calculations.

Samples. The samples of $DyBr_3$ used for the ED, MI-IR, and MI-Ra experiments were provided by Philips Lighting B.V., Eindhoven, The Netherlands (99.9% purity, specified on the metal basis. Additional anion impurity is oxygen, about 200−400 ppm.). The sample of $DyBr_3$ for the gas phase IR experiment was purchased from Cerac (99.9% purity of the compound). All chemicals were used without further purification as X-ray diffraction analysis showed the samples to be phase pure.

Electron Diffraction Experiment and Structure Analysis. The electron diffraction patterns were recorded at 1170(50) K with the Budapest EG-100A apparatus,[49,50] using a high-temperature molybdenum nozzle[51] and 60 kV accelerating voltage. Further details of the experiment and the experimental electron diffraction molecular intensities are given in the Supporting Information, Table S2. The molecular intensities and radial distributions are shown in

(26) Simons, J. *J. Phys. Chem.* **1989**, *93*, 626–627.
(27) Werner, H. J. *Mol. Phys.* **1996**, *89*, 645–661.
(28) Werner, H. J.; Celani, P. *J. Chem. Phys.* **2000**, *112*, 5546–5557.
(29) Berning, A.; Schweizer, M.; Werner, H. J.; Knowles, P. J.; Palmieri, P. *Mol. Phys.* **2000**, *98*, 1823–1833.
(30) Varga, Z.; Lanza, G.; Minichino, C.; Hargittai, M. *Chem.−Eur. J.* **2006**, *12*, 8345–8357.
(31) Cundari, T. R.; Stevens, W. J. *J. Chem. Phys.* **1993**, *98*, 5555–5565.
(32) Dolg, M.; Stoll, H.; Savin, A.; Preuss, H. *Theor. Chim. Acta* **1989**, *75*, 173–194.
(33) Dolg, M.; Stoll, H.; Preuss, H. *J. Chem. Phys.* **1989**, *90*, 1730–1734.
(34) Cao, X. Y.; Dolg, M. *J. Mol. Struct.:THEOCHEM* **2002**, *581*, 139–147.
(35) Yang, J.; Dolg, M. *Theor. Chem. Acc.* **2005**, *113*, 212–224.
(36) Dolg, M. PhD Thesis, University of Stuttgart, Stuttgart, Germany, 1989.
(37) Peterson, K. A.; Figgen, D.; Goll, E.; Stoll, H.; Dolg, M. *J. Chem. Phys.* **2003**, *119*, 11113–11123.
(38) Foster, J. P.; Weinhold, F. *J. Am. Chem. Soc.* **1980**, *102*, 7211–7218.
(39) Glendening, E. D.; Reed, A. E.; Carpenter, J. E.; Weinhold, F. NBO 3.1, 1998.
(40) Reed, A. E.; Curtiss, L. A.; Weinhold, F. *Chem. Rev.* **1988**, *88*, 899–926.
(41) Reed, A. E.; Weinstock, R. B.; Weinhold, F. *J. Chem. Phys.* **1985**, *83*, 735–746.
(42) Wiberg, K. *Tetrahedron* **1968**, *24*, 1083.
(43) Bergner, A.; Dolg, M.; Kuchle, W.; Stoll, H.; Preuss, H. *Mol. Phys.* **1993**, *80*, 1431–1441.
(44) Nicklass, A.; Dolg, M.; Stoll, H.; Preuss, H. *J. Chem. Phys.* **1995**, *102*, 8942–8952.
(45) Werner, H. J. et al. *MOLPRO*; 2006; For full reference, see Supporting Information.
(46) Frisch, M. J. et al. *Gaussian 98*, 1998; For full reference, see Supporting Information.
(47) Frisch, M. J. et al. *Gaussian 03*, 2003; For full reference, see Supporting Information.
(48) Schmidt, M. W. et al. *Gamess*, 1993;For full reference, see Supporting Information.
(49) Hargittai, I.; Tremmel, J.; Kolonits, M. *HIS, Hung. Sci. Instrum.* **1980**, *50*, 31–42.
(50) Hargittai, I.; Bohatka, S.; Tremmel, J.; Berecz, I. *HIS, Hung. Sci. Instrum.* **1980**, *50*, 51–56.
(51) Tremmel, J.; Hargittai, I. *J. Phys. E. Sci. Instrum.* **1985**, *18*, 148–150.

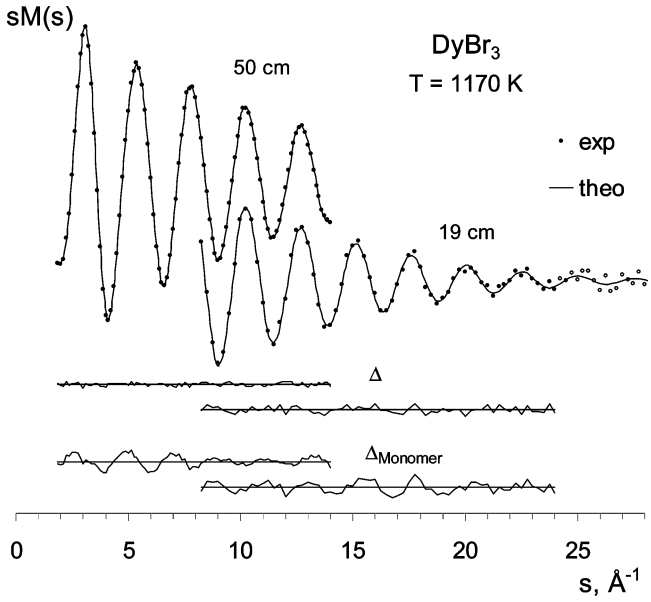

Figure 1. Experimental and calculated electron diffraction molecular intensities and their differences (Δ) for dysprosium tribromide. The difference for the "only monomer" theoretical intensities is also indicated.

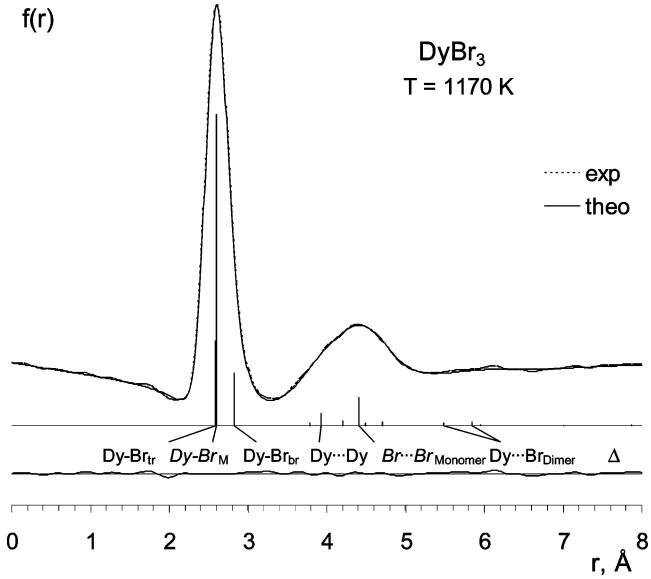

Figure 2. Experimental and calculated radial distribution curve and their difference (Δ) of dysprosium tribromide from electron diffraction. The contributions of different bond lengths and non-bonded distances are indicated (M: monomer, the rest are distances of the dimer; tr: terminal, br: bridging bond length).

Figures 1 and 2, respectively. The electron scattering factors were taken from ref 52.

On the basis of the results of the mass spectrometric study,[18] the presence of dimers was checked in the ED analysis, even if, according to the radial distribution curve (see Figure 2), the concentration of dimers cannot be high in the vapor. Therefore, certain constraints about its structure had to be applied in the analysis. At the first stage of the analysis, the difference of the monomer and the dimer terminal bond lengths, the difference between the two dimer bond lengths, and the bond angles of the dimer were taken from the MP2 basis **B** computations. For the analysis, the computed equilibrium bond length differences were converted to the "r_a" operational parameter with proper anharmonic corrections (vide infra). The vibrational amplitudes of both monomers and dimers were calculated by a normal coordinate analysis using the program ASYM20,[53] based on the computed force fields and frequencies. For the monomer, the normal coordinate analysis was also carried out based on the experimental gas-phase frequencies. These calculated amplitudes were used as starting parameters in the ED analysis but later on most of them were refined in groups. Stretching anharmonicity is also an important characteristic of metal halides.[6] To get some preliminary information about this parameter, the Morse constant was estimated based on our calculation of the DyBr molecule.

The vapor composition and all parameters of the monomeric $DyBr_3$ molecule were refined. The dimer was treated as a C_{2v}-symmetry molecule because of the thermal-average nature of the electron diffraction geometry. The ED analysis is especially sensitive to the low-frequency out-of-plane vibrations; therefore, we carried out an anharmonic analysis for the puckering frequency of the monomeric molecule.

Constraining the different bond-length differences and the bond angles of the dimer based on the computation gave a relatively good agreement with the experiment—but not a perfect one. Therefore, we also tried to refine some of these parameters. Constraining the bond length differences and refining the dimer bond angles gave a good agreement with experiment (see Figures 1 and 2). All parameters in the final refinement are realistic and considering the fact that the ED structure is a thermal average structure, the difference between the bond angles of the equilibrium versus average structures is acceptable, especially since the final values agree with the computed ones within their—rather large—experimental uncertainty.

Vibrational Spectroscopic Experiments. The gas-phase IR spectra were recorded with a Bomem DA3.02 Fourier-transform spectrometer equipped with an optical gas-cell (HTOC-2) constructed at ECN.[54,55] The spectra were recorded between 1190 and 1370 K at 0.5 cm^{-1} resolution; 128 scans were co-added.

The apparatus for the matrix-isolation experiments consisted of a Displex DE 202 cryotip (Air Products and Chemicals, Allentown, PA), which can be rotated in a homemade stainless steel vacuum shroud. The temperature of the deposition window was usually in the range of 14−17 K during formation of the matrixes. The detailed description of the matrix-isolation equipment is given in ref 56. The $DyBr_3$ evaporations were performed in the temperature range 1030−1170 K; deposition times varied between 15−320 min.

The IR spectra of matrix-isolated species were recorded in reflection mode with a Bomem DA3.02 Fourier-transform spectrometer equipped with a Bomem APG 7400D mirror bench. Resolution was 0.5 cm^{-1} or better; 256 scans were co-added. Raman spectra were measured using a Dilor Modular XY spectrometer coupled to a CCD detector (Wright Instruments Ltd.) or a multichannel diode array detection system. Since different optical windows had to be fitted upon changing from IR to Raman measurements, it was impossible to measure the Raman and IR spectrum of the same matrix. Further technical details of the

(52) Ross, A. W.; Fink, M.; Hilderbrandt, R.; Wang, J.; Smith, V. H. J. In *International Tables for X-Ray Crystallography*; Wilson, A. J. C., Ed.; Kluwer: Dordrecht, 1995; Vol. C, p 245.
(53) Hedberg, L.; Mills, I. M. *J. Mol. Spectrosc.* **1993**, *160*, 117–142.
(54) Konings, R. J. M.; Booij, A. S.; Cordfunke, E. H. P. *Vib. Spectrosc.* **1991**, *1*, 383–387.
(55) Konings, R. J. M.; Booij, A. S. *J. Chem. Thermodyn.* **1992**, *24*, 1181–1188.
(56) Groen, C. P. PhD Thesis, University of Amsterdam, Amsterdam, The Netherlands, 2009.

Table 1. CASSCF, CASPT2, MRCI+Q, and CASSCF-SO Optimized Geometries of the Lowest-Lying Electronic States of $DyBr_3$ and their Energy Differences[a]

state	$r(Dy-Br)_1$[b]	$r(Dy-Br)_2$[b]	Br−Dy−Br	ΔE
		CASSCF, C_{2v}		
$^6B_1$	2.6507	2.6507	120.0	0.00
$^6A_1$	2.6509	2.6506	119.3	0.50
$^6B_2$	2.6505	2.6508	120.7	0.50
$^6A_2$	2.6512	2.6504	120.1	2.34
$(2)^6B_1$	2.6501	2.6510	119.9	2.34
		CASPT2, C_{2v}		
$^6B_1$	2.5743	2.5740	120.0	0.00
$^6A_1$	2.5720	2.5756	118.1	0.71
$^6B_2$	2.5733	2.5723	121.4	1.71
$^6A_2$	2.5740	2.5717	120.2	6.48
$(2)^6B_1$	2.5732	2.5761	119.9	2.13
		MRCI+Q, D_{3h}		
$^6A_2''$	2.6008	2.6008	120.0	0.00
$^6E'$	2.6008	2.6008	120.0	0.54
$^6E''$	2.6008	2.6008	120.0	3.05
		MRCI+Q, C_{2v}		
$^6B_1$	2.6008	2.6008	120.0	0.00
$^6A_1$	2.6004	2.6010	119.0	0.46
$^6B_2$	2.6010	2.6007	120.9	0.46
$^6A_2$	2.6019	2.6003	120.2	3.05
$(2)^6B_1$	2.5996	2.6013	119.8	3.01
		CASSCF-SO[c]		
1	2.6508	2.6508	119.99	0.00
2	2.6509	2.6509	120.00	0.63
3	2.6509	2.6509	119.99	2.05
4	2.6509	2.6509	119.99	6.60

[a] Bond lengths in Å, angles in deg, relative energies in kJ/mol. [b] Two different bond lengths of a Jahn−Teller distorted C_{2v}-symmetry molecule. [c] All states are 2-fold degenerate.

spectroscopic experiments can be found in the Supporting Information.

Results

Molecular Geometry. $DyBr_3$ Monomer. Optimized geometrical parameters and relative energies for D_{3h} and C_{2v} symmetry structures are given in Table 1 at the CASSCF, CASPT2, and MRCI+Q levels of theory for the lowest-lying electronic states of $DyBr_3$. In all these calculations Basis **C** was applied with diffuse functions on the bromine atoms (aug-cc-pVTZ-PP). Since these states differ only in their Dy 4f occupation, it is perhaps not surprising that the geometries are nearly identical for the different states. This is also consistent with our previous $DyCl_3$ results[13] at this level of theory. As shown in Table 1, the ground state of the monomer is calculated to have a D_{3h} symmetric structure, $^6A_2''$ (note that computations in C_{2v}-symmetry also optimized to this structure). For the lower excited states (with energies only slightly higher than that of the ground state) the energies and structural parameters of the constrained D_{3h} and (unconstrained) C_{2v} structures differ only very slightly, by at most about 0.002 Å, 1.0°, and 0.08 kJ/mol for the bond lengths, angles, and excitation energies, respectively. The importance of electron correlation is well seen from Table 1, in that the MRCI+Q bond lengths are about 0.05 Å shorter than the ones from the CASSCF calculations. The excitation energies, however, are changed only slightly. The CASPT2 method appears to overestimate the effects of electron correlation, yielding bond lengths systematically too short by about 0.03 Å.

Table 2. Vertical Excitation Energies (in kJ/mol) of $DyBr_3$ at the MRCI+Q Level of Theory Calculated at the $^6A_2''$ MRCI+Q Equilibrium Geometry

	$n = 1$	$n = 2$	$n = 3$	$n = 4$
$(n)^6E'$	0.75	16.78	82.30	339.41
$(n)^6A_2''$	0.00	82.38	357.23	
$(n)^6E''$	3.64	12.97	82.47	
$(n)^6A_1'$	7.41	69.75		
$(n)^6A_2'$	7.15	77.99		

The vertical excitation energies of $DyBr_3$ calculated at the MRCI+Q level of theory relative to the $^6A_2''$ ground electronic state are given in Table 2. There are six excited electronic states within 17 kJ/mol of the ground state and the $(1)^6E'$ state has an excitation energy of just 0.75 kJ/mol. The next manifold of sextet states lies about 70−85 kJ/mol above the ground state. Not shown in Table 2 are the numerous quartet states that lie about 305 kJ/mol (CASSCF level of theory) above the ground state.

The importance of using CAS-based calculations for such systems is shown by the following: trial UHF calculations were carried out in C_{2v}-symmetry to see the possible effect of Jahn−Teller distortion on the geometries.[57] We tried different occupations of the seven 4f orbitals with the 9 electrons of Dy and found that, indeed, the minimum-energy geometry appeared to be a Jahn−Teller distorted C_{2v}-symmetry structure. In these calculations the lowest-energy D_{3h}-symmetry excited state ($^6A_2''$) appeared to be about 17 kJ/mol higher in energy than the C_{2v}-symmetry ground state. However, we have to emphasize, that it is *not a good approach* to use UHF-based methods to determine the symmetry of these types of molecules.[13] In such calculations—obviously these comments apply only to calculations in which the 4f electrons are part of the valence shell—the chosen unsymmetrical 4f occupation artificially removes the spatial symmetry of the electronic wavefunction and thus a C_{2v}-symmetry structure might result for molecules in degenerate electronic states. On the other hand, the CASSCF calculations take into consideration all possible occupancies in the given active space, and give reliable results as far as the symmetry of the electronic state is concerned. As discussed above, all our CASSCF and MRCI+Q calculations resulted in a D_{3h}-symmetry geometry for the ground state, even if the optimization was carried out in C_{2v}-symmetry (see Table 1). The ground electronic state then is nondegenerate with $^6A_2''$ symmetry. The first two excited states are nearly degenerate, corresponding to a Jahn−Teller distorted $^6E'$ state, with an only slightly higher energy (0.46 kJ/mol) than the ground state, and slightly distorted structures with $^6A_1$ and $^6B_2$ symmetries. The third and fourth excited states are only about 3 kJ/mol above the ground state and correspond to a Jahn−Teller-distorted $^6E''$ state (leading to $^6A_2$ and $^6B_1$ C_{2v} symmetry states, see Table 1).

The dominant effect of including spin−orbit coupling into the calculations is to completely quench the Jahn−Teller distortions in all the low-lying electronic states (see Table

(57) Jahn, H. A.; Teller, E. *Proc. R. Soc. London.Ser.A* **1937**, *161*, 220–235.

Table 3. Effect of Basis Set and Correlation Treatment on the Bond Length of $DyBr_3$ and Experimental Equilibrium Bond Length (Å)

	corr. level[a]		
method/basis[b]	FC	G2	G2 + 3d
MP2/A	2.664	2.637	
MP2/B	2.596	2.580	
MP2/C	2.581	2.571	
CASPT2/C+2d2f		2.573	2.562
MRCI+Q/C		2.601	2.590[c]
Electron Diffraction			
r_e^{Md}	2.591(8)		
r_e^{Md} ref 19	2.591(5)		

[a] FC: frozen core (correlating 6s, 5d for Basis **A** and 6s, 4f for Bases **B** and **C** on Dy), G2: as in FC but the 5s, 5p electrons of Dy are also included in the correlation calculation, G2 + 3d: the 3d electrons of Br were included (Basis C was augmented with additional tight functions - see the Computational section). [b] For description of bases see the Computational section and Supporting Information. [c] Using the correction obtained from the CASPT2 calculations. [d] Estimated experimental equilibrium bond length; calculated from the thermal-average bond length, r_g (see Table 4), by Morse-type anharmonic vibrational corrections, $r_e \approx r_g - 3al^2/2$, where a is the Morse constant and l is the vibrational amplitude of the bond length at the temperature of the experiment.

1). It has a negligible effect on the ground-state structure. In addition, the excitation energies form a relatively regular progression with the first 65 spin−orbit coupled states lying within just 130 kJ/mol of the ground state. All states have essentially identical bond lengths of about 2.651 Å at the CASSCF level of theory (see Table 1).

Further computations have been carried out at the MP2 level of theory with different basis sets for both the monomeric and dimeric molecules. The monomer results are given in Table 3, together with the estimated experimental equilibrium bond length. Two different correlation treatments were checked with all three basis set combinations; the frozen core (FC) and the "FreezeG2" option of the Gaussian program packages. The FC calculation correlates only the electrons of the valence shell (meaning $6s^25d^1$ for Basis **A** and $6s^24f^{10}$ for Bases **B** and **C** on the Dy atom). The FreezeG2 option, on the other hand, also correlates the 5s and 5p electrons of Dy but still leaving the 3d electrons of Br frozen.

As already mentioned above, the importance of electron correlation is obvious; as the comparison of the CASSCF and MRCI+Q calculations also showed. Apparently, of similar importance is the inclusion of the electrons of the $n = 4$ and 5 shells in the valence shell—all large-core calculations (Basis **A**) produced much too long bond lengths. The most striking difference is observed when going from Basis **A** to Basis **B** (Stuttgart LC to Cundari); the bond length decreases by about 0.06−0.07 Å. The difference between the two cases is basically the inclusion of the 4f electrons in the core (Stuttgart LC) versus in the basis set (Cundari); thus we may draw the conclusion that including the 4f orbitals in the valence shell is important if we want to get reliable geometrical parameters. On further moving from Basis **B** to Basis **C** the bond length shortens only by about 0.01 Å. The Stuttgart SC calculations (Basis **C**) produced somewhat shorter bond lengths than the experimental ones at the MP2 level of theory. We have to mention though that we had similar experience with our work on $DyCl_3$, where the SC MP2 calculations resulted in too short bond lengths, but the same level CCSD(T) calculations gave very good results. For $DyBr_3$ we were not able to carry out CCSD(T) level computations because of strong configurational mixing. The effect of correlating the Br 3d electrons at the CASPT2 level of theory with the modified Basis **C** is to decrease the bond length by 0.011 Å. As shown in Table 3, when this result is combined with the MRCI+Q equilibrium bond length (G2 core) excellent agreement with experiment is obtained.

Table 4. Results of the Electron Diffraction Analysis[a]

	r_g (Å), $\angle_a$ (deg)	l (Å^{-1})	κ (Å^3)
	Monomer		
Dy−Br	2.606(8)[b]	0.093(4)[c]	4.4(10) × 10^{-5}
Br···Br	4.428(64)	0.316(29)	
$\angle^d$	115.6(2.1)		
$\angle_e{}^e$	114.6		
	Dimer		
$\Delta(M-D_t)^f$	[0.018]		
$\Delta(D_b-D_t)^g$	[0.220]		
$Dy-Br_t{}^h$	2.589(10)	0.096(4)[c]	5.1(10) × 10^{-5}
$Dy-Br_b{}^i$	2.832(20)	0.141(4)[c]	2.5 × 10^{-4}[j]
$\angle(Br_t-Dy-Br_t)$	120(17)		
$\angle(Br_b-Dy-Br_b)$	84(5)		
$\%_{dimer}$	17(4)		
R_f (%)[k]	4.18		

[a] r_g - thermal average distance at 1170 K. Error limits are estimated total errors, including systematic errors, and the effect of constraints used in the refinement: $\sigma_t = (2\sigma_{LS}^2 + (c \cdot p)^2 + \Delta_i^2)^{1/2}$, where σ_{LS} is the standard deviation of the least-squares refinement, p is the parameter, c is 0.002 for distances and 0.02 for amplitudes and Δ_i are the effect of different constraints. l is the vibrational amplitude and κ the asymmetry parameter. [b] 2.609(5) ref 19. [c] Refined in one group. [d] Thermal average bond angle from ED. [e] Estimated thermal average bond angle from computation based on the anharmonic analysis of the puckering vibration. [f] Difference of monomer and dimer terminal bond lengths, in r_e representation. Value taken from the computations and transformed to r_a operational parameters and constrained during refinement. [g] Difference of dimer bridging and terminal bond lengths, in r_e representation. Value taken from the computations and transformed to r_a operational parameters and constrained during refinement. [h] Terminal bond length of the dimer. [i] Bridging bond length of the dimer. [j] Not refined. [k] Goodness of fit.

Because of the controversies about the shape of lanthanide trihalides from experiments, D_{3h} versus C_{3v}, vide supra, we also checked the possibility of a C_{3v}-symmetry pyramidal geometry. All these optimizations ended up with a D_{3h}-symmetry geometry. Electron diffraction gives a thermal averaged structure, which appears to be pyramidal because of the low-frequency, large amplitude puckering vibration of even a planar molecule. Our thermal average bond angle is 115.6(2.1)° (Table 4), in agreement with the results of ref 19. We also estimated the thermal average angle from computations by an anharmonic analysis of the puckering vibration. This gave us a 114.6° angle, in good agreement with the electron diffraction results.

The NBO analysis of the monomer shows that the bonding in the monomeric molecule is highly ionic with a partial charge of 2.37e on dysprosium. According to the population analysis, Dy [core]6s(0.18)4f(8.93)5d(0.45)6p(0.04), there is only a small amount of s electrons left on Dy, also verifying the ionic character. The Wiberg bond index is 0.36. All the covalent bonding is the result of the overlap between the dysprosium 5d and the bromine 4p electrons, similar to the case of $DyCl_3$.[13]

Dy_2Br_6 Dimer. On the basis of our previous CASSCF results for the Dy_2Cl_6 system,[13] CASSCF (18 electrons in

Table 5. Calculated Geometrical Parameters and Relative Energies of Dy_2Br_6 for the Lowest Electronic States[a]

method/basis[b]	corr. level[c]	electronic state	ΔE	Dy−Br_t	Dy−Br_b	Br_t−Dy−Br_t	Br_b−Dy−Br_b
MP2/**A**	FC	$^{11}B_{3u}$		2.650	2.871	117.5	86.1
	FC1	$^{11}B_{3u}$		2.615	2.820	117.9	86.9
MP2/**B**	FC	$^{11}B_{3u}$		2.582	2.799	117.4	86.7
	G2	$^{11}B_{3u}$		2.564	2.771	115.8	87.6
MP2/**C**	FC	$^{11}B_{3u}$		2.566	2.775	115.8	87.4
	FC1	$^{11}B_{3u}$		2.538	2.730	115.5	88.7
CASSCF							
high-spin		$^{11}B_{2g}$, $^{11}B_{1u}$	0.00	2.643	2.871	120.1	85.5
		(2×)$^{11}B_{3u}$, $^{11}B_{3g}$, $^{11}A_u$	6.2	2.642	2.870	116.3	84.8
		$^{11}B_{1g}$, $^{11}B_{2u}$	16.4	2.642	2.871	118.7	85.2
		$^{11}A_g$	20.0	2.643	2.870	118.2	85.1
low-spin		$^{1}A_g$, $^{1}B_{2g}$, $^{1}B_{1u}$	0.00	2.643	2.870	120.1	85.5
		$^{1}B_{3g}$, $^{1}A_u$	6.2	2.642	2.870	116.3	84.8
		$^{1}B_{1g}$, $^{1}B_{2u}$	16.4	2.642	2.872	118.6	85.2
		$^{1}B_{3u}$	20.0	2.642	2.780	118.2	85.1

[a] Bond lengths in Å, angles in deg., energies in kJ/mol. [b] For description of bases see the Computational section and Supporting Information. [c] See the footnote to Table 3.

14 orbitals) geometry optimizations were also carried out for several low-lying high-spin (undecuplet) electronic states of the $DyBr_3$ dimer. These results, shown in Table 5, are remarkably similar to those reported for Dy_2Cl_6. In particular, there are groups of isoenergetic states with very similar molecular geometries. As in Dy_2Cl_6 the high spin ground state of Dy_2Br_6 consists of the $^{11}B_{2g}$ and $^{11}B_{1u}$ pair. There are four isoenergetic states about 6.2 kJ/mol higher in energy: (1)$^{11}B_{3u}$, (2)$^{11}B_{3u}$, $^{11}B_{3g}$, and $^{11}A_u$ states, corresponding to the first excited state. On the other hand, in our UHF-MP2 calculations the $^{11}B_{3u}$ electronic state was the lowest-energy state that was amenable to this method, as discussed in ref 13. The results of these MP2 geometry optimizations for the ground-state dimer molecule, with all three basis sets, are given in Table 5 and, after comparison with the $DyBr_3$ monomer results (see Table 3), are entirely consistent with the CASSCF results for this state. The molecule has a D_{2h}-symmetry structure, with two halogen bridges; this is the usual structure of metal trihalide dimers.[6]

Calculations were also carried out on the low-spin singlet states of the dimer (see Table 5). For six states, the energies and geometries are essentially the same as for the undecuplet states, while there are two electronic states that behave differently. For the singlets, the $^{1}A_g$ state is (one of) the ground states, and the $^{1}B_{3u}$ state is the highest in energy among the ones shown in Table 5, while the situation is more or less reversed for the high-spin states. The fact that the high-spin and low-spin states have about the same energy is surprising considering Hund's rule and might be an indication of an antiferromagnetic coupling between the two metal centers in the dimer. A similar situation was found in the dimer of $DyCl_3$.[13] Antiferromagnetic coupling has been observed experimentally at low temperatures for lanthanide complexes earlier, for example, in the halide complexes of $DyBr_3$,[58] even if it is usually weaker than the same effect in transition metal complexes because of the inner nature of the f orbitals. We have also recently observed antiferromagnetic coupling in the dimers of $CrCl_2$.[59]

As discussed above, the vapors of $DyBr_3$ contain a relatively small but noticeable amount of dimers. In spite of their small amount, we could determine its structure, even if with a large uncertainty, from electron diffraction as shown in Table 4. The situation was luckier than in case of $DyCl_3$; we had a larger range of experimental intensity data here, and the larger scattering power of the bromine atoms also helped.

Vibrational Spectroscopy. The vibrational spectra of $DyBr_3$ were measured by applying gas-phase IR, MI-IR, and MI-Ra spectroscopy. A summary of the analysis of the spectra and the derivation of recommended harmonic gas phase values is given here. A more detailed account of the vibrational spectroscopic results can be found in the Supporting Information. The IR spectrum of the $DyBr_3$ vapor at about 1245 K is shown in Figure 3. Under the observed band contours the calculated (MP2/Basis **B**) IR spectra of both $DyBr_3$ and Dy_2Br_6 are shown. The observed and computed frequencies (with their infrared intensities) are given in Tables 6 ($DyBr_3$) and 7 (Dy_2Br_6).

The broad band dominating the stretching region of the spectrum at 243 cm^{-1} can be assigned to the Dy−Br asymmetric stretching fundamental ν_3 that must be influenced by the excited vibrational and rotational modes at the high temperature of the experiment. This influence was assessed on the basis of calculations done on the reference system $GdBr_3$ (Supporting Information, Table S3). The evaluation of the effect of thermal averaging over all the excited vibrational levels is given in the Supporting Information, leading to a value of 245 cm^{-1} for the ν_3 fundamental of $DyBr_3$.

The presence of dimers is indicated by the broad absorption around 156 cm^{-1} in the experimental gas-phase spectrum. No monomer absorption is expected in this spectral region, while two IR active dimer fundamentals are computed to have considerable IR intensity in this part of the spectrum (see Table 7). On the basis of the computed frequencies, we assign our observed band contour around 156 cm^{-1} to the asymmetric Dy−Br ring stretches of Dy_2Br_6, calculated at 155.1 cm^{-1} (B_{3u}) and 175.1 cm^{-1} (B_{1u}) (MP2/Basis **B**). The observation of these two vibrations implies that the two dimer Dy−Br terminal stretches, with even higher calculated IR

(58) Schilling, G.; Bocker, M.; Moller, A.; Meyer, G. *Z. Anorg. Allg. Chem.* **2001**, *627*, 1309–1312.

(59) Vest, B.; Varga, Z.; Hargittai, M.; Hermann, A.; Schwerdtfeger, P. *Chem.—Eur. J.* **2008**, *14*, 5130–5143.

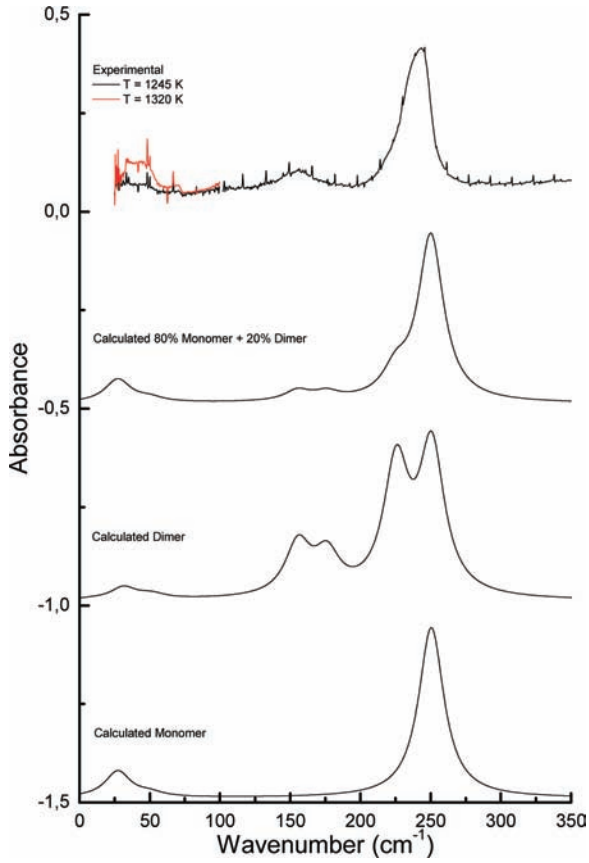

Figure 3. IR spectrum of the vapor above $DyBr_3$ at 1245 K. The bending region (25−100 cm^{-1}) is also shown for a temperature of 1320 K (red upper trace). The computed spectra of a mixture of 80% monomer and 20% dimer, the dimer, and the monomer spectra (calculated with Basis **B**) are also plotted. The conversion of the calculated fundamental frequencies to a synthetic IR spectrum is done by the GaussView program, applying a full-width at half-maximum for all the fundamentals of 22 cm^{-1}. This value has been derived from the experimental $DyBr_3$ ν_3 fundamental.

Table 6. Computed Harmonic Vibrational Frequencies (cm^{-1}, with IR Intensities [km mol^{-1}] in Parentheses) and Experimental Vibrational Frequencies for $DyBr_3$ ($^6A_2''$)

method/basis[a]	ν_1	ν_2	ν_3	ν_4
MP2/**A**, FC1	200.1 (0)	27.4 (20)	247.8 (126)	48.0 (2)
MP2/**A**, FC	195.4 (0)	30.0 (20)	242.1 (134)	47.6 (2)
MP2/**B**, FC	200.2 (0)	26.9 (21)	250.1 (134)	49.7 (4)
MP2/**C**, FC	202.5 (0)	20.5 (18)	253.7 (124)	50.5 (2)
IR (gas)[b]		41	243	50
MI(Ar)-IR ref 20			243.1	
MI(Kr)-IR	211.5		237.2	
MI(Kr)-Raman	211		237	
MI(Xe)-IR	206.1		229.4	
MI(Xe)-Raman	206		230	52
recommended harmonic gas-phase values	204 ± 7	35 ± 5	245 ± 5	50 ± 5

[a] For notations see footnote to Table 3 and for description of bases see Computational Section and Supporting Information. [b] The tabulated gas-phase frequencies are the bands observed in the spectrum at 1245 K without correction for excited vibrational and rotational modes at the temperature of the experiment.

intensities, should also be present in the spectrum. The calculated asymmetric dimer Dy−Br terminal stretch (B_{2u}) at 252.3 cm^{-1}, coincides with the computed vibrational frequency for the monomer ν_3 (250.1 cm^{-1}); thus, it will not be observable as a separate band or shoulder. The presence of the dimer symmetric Dy−Br terminal stretch

Table 7. MP2 Harmonic Vibrational Frequencies (cm^{-1}, with IR Intensities [km mol^{-1}] in Parentheses) and Experimental Vibrational Frequencies for Dy_2Br_6 ($^{11}B_{3u}$)

symmetry	mode	character[a]	MP2(FC)/**B**	IR (gas)
A_g	ν_1	ν_s Dy−Br_t	235.5 (0)	
	ν_2	ν_s Dy−Br_b	162.1 (0)	
	ν_3	β_s Br_b−Dy−Br_b	76.5 (0)	
	ν_4	β_s Br_t−Dy−Br_t	37.3 (0)	
A_u	ν_5	δ_{as} Br_t−Dy−Br_t	23.7 (0)	
B_{1g}	ν_6	ν_{as} Dy−Br_t	248.4 (<1)	
	ν_7	β_{as} Br_t−Dy−Br_t	27.1 (0)	
B_{1u}	ν_8	ν_{as} Dy−Br_b	175.1 (26)	170 ± 10
	ν_9	δ_s Br_t−Dy−Br_t	28.3 (10)	
B_{2g}	ν_{10}	ν_{as} Dy−Br_b	129.1 (0)	
	ν_{11}	δ_{as} Br_t−Dy−Br_t	39.7 (0)	
B_{2u}	ν_{12}	ν_{as} Dy−Br_t	252.3 (115)	245 ± 5
	ν_{13}	ring puckering	55.8 (1)	
	ν_{14}	θ Dy−Br_b−Dy−Br_b	8.2 (<1)	
B_{3g}	ν_{15}	ring twist	31.3 (0)	
B_{3u}	ν_{16}	ν_s Dy−Br_t	224.6 (98)	220 ± 10
	ν_{17}	ν_{as} Dy−Br_b	155.1 (41)	155 ± 10
	ν_{18}	β_{as} Br_t−Dy−Br_t	47.3 (3)	

[a] The symbols or abbreviations ν, β, δ, θ, s, as mean stretch, in-plane bend, out-of-plane bend, torsion, symmetric and asymmetric, respectively.

(B_{3u}), calculated at 224.6 cm^{-1}, is indicated by the asymmetrical appearance of the monomer ν_3 band in which a shoulder can be recognized at about 220 cm^{-1}. The presence of this signal in the low-wavenumber wing of the monomer ν_3 stretch band might have a small influence on the observed band maximum for the monomer ν_3 by shifting it to lower wavenumbers compared to the actual value. This effect is accounted for in the uncertainty of the recommended gas-phase value for this fundamental (245 ± 5 cm^{-1}).

The bending region (25−100 cm^{-1}) has a complex band between 30 and 60 cm^{-1}. On the basis of the computed IR intensities, the ν_2 out-of-plane mode of the monomer is the major contributor to this region, for which the high population of excited vibrational and rotational levels causes considerable anharmonicity. The way the anharmonicity was derived is given in the Supporting Information. We determined a negative anharmonicity constant of 0.5 cm^{-1} for the 1 → 2 hot band decreasing to 0.2 cm^{-1} for the hot bands above 15 → 16 (see Supporting Information, Table S4). Weighting the v → v+1 transitions by their Boltzmann distribution gives an average anharmonic frequency of 33.5 cm^{-1} at the temperature of our experiment, an increase of 6 cm^{-1} with respect to the anharmonic fundamental transition 0 → 1. To obtain the experimental value of ν_2 corrected for anharmonicity, we have taken the center of the broad absorption at 41 cm^{-1} and subtracted from this the computed anharmonic correction of 6 cm^{-1}. This results in an experimental value for ν_2 of 35 cm^{-1} with an estimated uncertainty of 5 cm^{-1}.

Other signals with large-enough computed IR intensity that need be considered as minor contributors to the complex absorption in this region are the monomer ν_4 fundamental (computed at 49.7 cm^{-1}, Basis **B**) and the dimer deformation fundamental ν_9 (B_{1u}) computed at 28.3 cm^{-1}. The monomer ν_4 is located on the high wavenumber wing of the monomer ν_2 contour and tentatively might be assigned to the extra

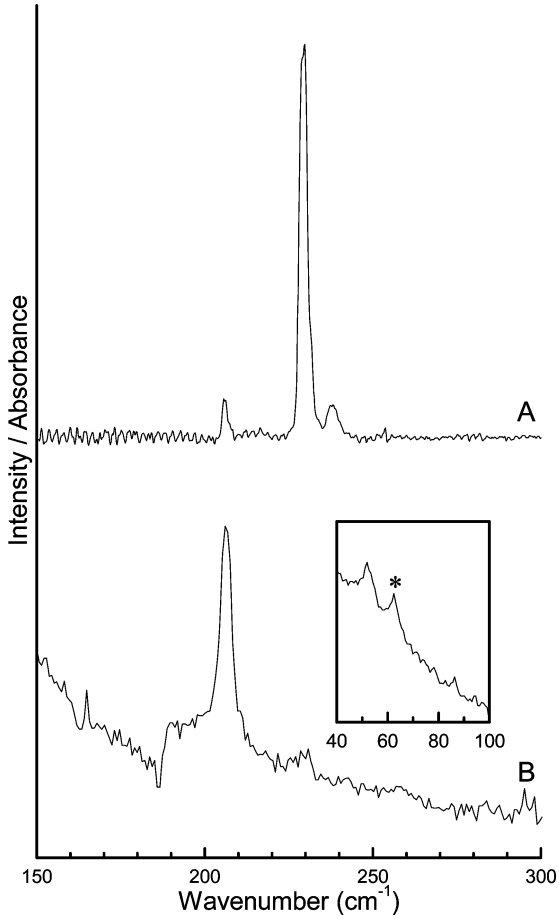

Figure 4. IR and Raman spectrum of matrix-isolated $DyBr_3$ in Xenon at 20 K. (A) IR spectrum, 65 min. deposition at $T = 1075(20)$ K. (B) Raman spectrum, 15 min. deposition at $T = 1075(20)$ K, $\lambda_{exc} = 514.5$ nm, laserpower = 400 mW. Inset: low-wavenumber region of the Raman spectrum. The signal denoted with an asterisk (*) is assigned to an impurity.

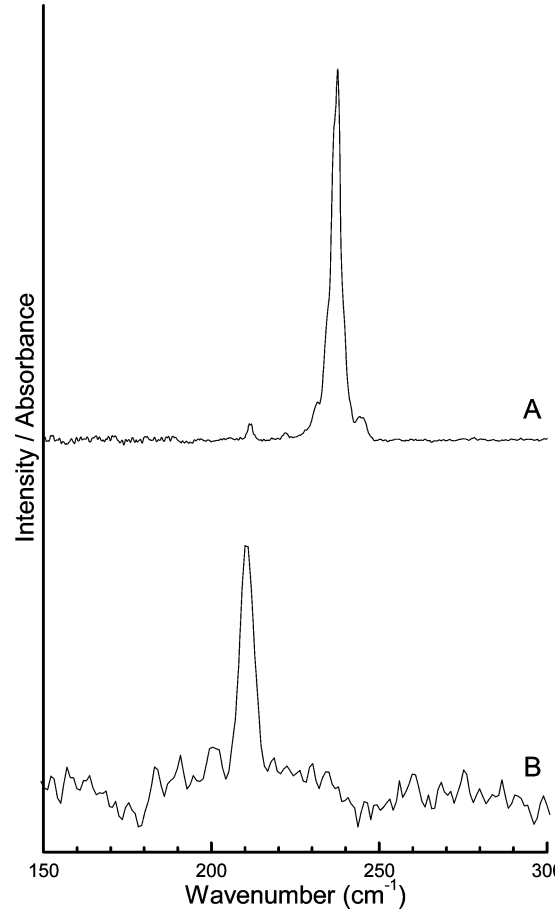

Figure 5. IR and Raman spectrum of matrix-isolated $DyBr_3$ in Krypton at 20 K. (A) IR spectrum, 320 min. deposition at $T = 1095(60)$ K. (B) Raman spectrum, 30 min. deposition at $T = 1145(20)$ K, $\lambda_{exc} = 514.5$ nm, laserpower = 400 mW.

intensity observed in the region around 50 cm^{-1}. The dimer ν_9 signal will most probably be hidden by the complex $\nu_2$band.

The MI-IR and MI-Ra spectra of $DyBr_3$ in xenon and krypton are shown in Figures 4 and 5, respectively. The IR spectra show one strong signal in the stretching region, located at 229.4 cm^{-1} in xenon and 237.2 cm^{-1} in krypton. This absorption is assigned to the asymmetric stretch fundamental, ν_3, of the monomer. An earlier argon matrix-isolation study determined the ν_3 at 243.1 cm^{-1}.[20] In the MI-Ra spectra the monomer ν_3 is also visible as a very weak signal at 230 $\pm$ 3 cm^{-1} (Xe) and 237 $\pm$ 3 cm^{-1} (Kr).

The strongest signals in the MI-Ra spectra of $DyBr_3$ in Xe (Figure 4B) and Kr (Figure 5B) appear at 206 $\pm$ 3 cm^{-1} and 211 $\pm$ 3 cm^{-1}, respectively. This signal is assigned to the monomer symmetric stretching frequency, ν_1. Interestingly, the symmetric stretching frequency seems to appear in the IR spectra as well, in xenon at 206.1 cm^{-1} and in krypton at 211.5 cm^{-1}. Under the wide variety of experimental conditions applied, these signals maintained a more or less constant intensity ratio with the monomer ν_3 absorption, suggesting that they originate from the same molecular species (see Supporting Information, Figure S1). The appearance of these signals in the MI-IR spectra implies that $DyBr_3$ adopts a pyramidal C_{3v} geometry in the matrix environments. To check this possibility, we placed the $DyBr_3$ molecules in an unsymmetrical cage of noble gas atoms and computed the structures. These computations (see Supporting Information, Table S5) showed that the molecular geometry of $DyBr_3$ changes from planar to pyramidal because of the formation of complexes with the matrix molecules, with their stabilization energies up to about -100 kJ/mol, depending on the number of coordinating noble gas atoms.

Deriving an estimated harmonic gas-phase value for the monomer ν_1 fundamental from the observed matrix-isolation frequencies is not a trivial task here. Usually, the observed frequencies are extrapolated to zero polarizability and that would be 221 $\pm$ 5 cm^{-1}. However, the fact that the symmetry of the $DyBr_3$ unit is different in the gas phase and in the matrixes does not allow a simple extrapolation. To estimate the gas-phase ν_1 fundamental from the MI spectra, we computed the structures of differently bent $DyBr_3$ molecules and their frequencies along the bending potential (see Supporting Information, Table S6). The table shows that there is an essentially linear relationship between the difference of ν_1 and ν_3 and the bond angle in the interval of 120 to 90 degrees. On the basis of this relationship from our measured data we estimate a 17 cm^{-1} decrease for the gas-phase value and thus the recommended harmonic gas-

phase value for the planar $DyBr_3$ molecule is $\nu_1 = 204 \pm 7$ cm^{-1}.

The 62 cm^{-1} signal in the MI-Ra spectrum appears to be an impurity, and this cannot be ruled out for the signal at 52 cm^{-1} either; although the latter might also be the in-plane deformation fundamental, ν_4, of monomeric $DyBr_3$. The IR signal with maxima at 237.6 cm^{-1} (Xe)/244.4 cm^{-1} (Kr) is probably due to a matrix site effect. Slightly heating the matrixes generally resulted in a decrease of this signal (see Supporting Information, Figure S3). That means that an interpretation in terms of a dimer band is unlikely as thermal diffusion generally enhances dimer formation.

Discussion

We determined the molecular geometry and vibrational frequencies of the gas-phase dysprosium tribromide molecule, both of its monomer and dimer, by high-level ab initio computations, electron diffraction, and three kinds of vibrational spectroscopic experiments. The electronic structure of the ground state and first few excited states of the monomer and dimer were also determined. An interesting aspect of the dimer structures is the nearly equal energies of the undecuplet and singlet electronic states that may suggest the possibility of antiferromagnetic behavior in the singlet.

The ground electronic state of the monomer is of $^6A_2''$ symmetry and the molecule is planar from all methods applied, even if the matrix-isolation experiments suggested pyramidal structures. Our computations of $DyBr_3$ placed in different krypton environments (see Supporting Information, Table S5) indicate that there is interaction between the $DyBr_3$ molecules and the surrounding matrix atoms, leading to the experimentally observed symmetry lowering. Thus, the appearance of the symmetric stretching fundamental in the MI-IR experiment is only due to the influence of the surrounding matrix, forcing the molecule to adopt a pyramidal structure. Similar observations have been made on other systems.[60] On the basis of our calculations of the effect of pyramidalization of $DyBr_3$, we estimated the gas-phase symmetric stretching frequency of the planar $DyBr_3$ molecule from our experimental matrix data.

According to our population analysis, the 4f orbitals of Dy do not participate in the bonding of the monomeric molecule, but their inclusion in the valence shell, together with the whole $n = 5$ shell, is essential to get reliable geometrical parameters from computation. An interesting and unexpected finding is that the bond angles of the dimer, especially the one involving the two terminal bromine atoms, are consistently different in their different electronic states, indicating the effect of different 4f orbital occupations on their geometry. We try to offer a possible explanation for this unanticipated result: The 4f orbitals are among the highest occupied nonbonding MOs. Inspection of these orbitals might explain the geometry differences between the different dimers: In one group (e.g., $^{11}A_u$), the $4f_{xz^2}$ orbital has a large contribution to the particular MO and because of the shape of this f orbital there is considerable charge density in the plane between the terminal bromine atoms that might push them apart, thus opening their bond angle. In another group (e.g., $^{11}B_{1u}$), the relevant 4f orbital is a $4f_{yz^2}$ orbital that has a nodal plane between the two terminal bromine atoms, and much of the charge density of the orbital is outside this region, thus it may push the bromines toward each other, thus closing their bond angle. The question might be asked: why do we not have similar effects in the monomer molecule? The monomer is planar; there such an effect is not expected because most of the charge density of the different nonbonding f orbitals is above and below the molecular plane. We think that the observed impact of 4f orbital occupation on the structure of the dimer could be a general phenomenon among the lanthanides that have a partially filled 4f shell (except for gadolinium with its half-filled 4f shell) that are surrounded by more than three ligands.

Our study, similarly to our previous experience with $DyCl_3$, demonstrated the importance of using multireference computations, such as CASSCF, for systems with partially filled orbitals, to determine the proper electronic states of the molecule. The use of single reference UHF-based methods may lead to erroneous results concerning the symmetry of the monomer molecule by producing an "unreal" lower-symmetry wave function. For a molecule like $DyBr_3$, such a calculation yields Jahn−Teller distorted C_{2v}-symmetry structures as the lowest-energy ones. The CASSCF calculations resulted in a nondegenerate ground electronic state of D_{3h} symmetry that is not even subject to the Jahn−Teller effect. As to the effect of spin−orbit coupling, its inclusion in the calculations quenches all of the small Jahn−Teller distortions, yielding only D_{3h}-symmetry structures.

As we already discussed in our paper on $DyCl_3$,[13] getting good structural parameters for a lanthanide trihalide does not come without a price. Obviously, the LC (here we only talk about the Dy basis set) calculations are the fastest, the geometry optimization of the monomer molecule takes less than half an hour, while the Cundari ECP calculations take about one hour and a half. The Stuttgart SC requires the longest time and computer performances; the optimization took almost one day. The frequency calculations take approximately 15 times longer computational time than the optimization procedures.[61]

Acknowledgment. M.H. and Z.V. acknowledge the support of the Hungarian Scientific Research Fund (OTKA K 60365) and the additional computational time from the National Information Infrastructure Development Program of Hungary. C.P.G. acknowledges the help of Mr. H. Luyten with developing the high temperature furnace for the matrix-isolation setup, Mr. A. S. Booij for his assistance with the gas-phase IR experiments, Mr. C. P. J. Groen for converting the data format from the gas-phase IR measurements, and Prof. E.H.P. Cordfunke and Prof. A. Oskam for their helpful comments and suggestions in the early stages of the

(60) Li, J.; Bursten, B. E.; Liang, B. Y.; Andrews, L. *Science* **2002**, *295*, 2242–2245.

(61) With a machine with a dual core CPU processor, about 8−16 Gbyte memory and around 2 GHz frequency.

vibrational spectroscopic work. The spectroscopic experiments were supported financially by STW (ACH 55.3757) and Philips Lighting B.V.

Supporting Information Available: Computational details, spectroscopic constants for the DyBr molecule (Table S1), details of the electron diffraction experiment, the molecular intensities at two different camera ranges (Table S2), PT2-VSCF anharmonic vibrational transitions of $GdBr_3$ (Table S3), population of excited vibrational levels for the out-of-plane vibration (Table S4), structural parameters and relative energies of the $DyBr_3 \cdot Kr_n$ complexes (Table S5), vibrational frequencies of differently bent $DyBr_3$ molecules (Table S6), technical details of the spectroscopic experiments and a detailed discussion of the vibrational spectroscopic analysis. This material is available free of charge via the Internet at http://pubs.acs.org.

IC802340G